RSC Advances

PAPER

View Article Online
View Journal | View Issue

Cite this: *RSC Adv.*, 2015, **5**, 18939

Two-dimensional colloidal crystal heterostructures†

Fei Xue,[a] Sanford A. Asher,*[b] Zihui Meng,*[a] Fengyan Wang,[a] Wei Lu,[a] Min Xue*[a] and Fenglian Qi[a]

Received 9th December 2014
Accepted 6th February 2015

DOI: 10.1039/c4ra16006a

www.rsc.org/advances

We developed a simple method to fabricate colloidal crystal heterostructures (CCHs) with two or three stacked poly(methyl methacrylate) (PMMA) particle two-dimensional (2D) colloidal monolayer arrays of different particle spacings that independently diffract light. The 2D colloidal monolayer arrays of PMMA were prepared by using the air/water interface self-assembly method we recently developed. Two- and three-layer CCHs were fabricated by successive deposition of 2D PMMA colloidal monolayer arrays of different particle sizes. The structure and optical properties of 2D monolayer arrays and 2D CCHs were characterized with SEM, reflectance spectra, their Debye diffraction rings and their diffracted wavelengths. The layers maintain their spacing and ordering as they are transferred from the air/water interface onto the substrate. The 2D CCHs diffraction measurements suggest that the optical properties of the colloidal crystal heterostructures arise mainly from the independent diffraction of the individual 2D colloidal arrays. This enables selective combination of particular light wavelengths through diffraction of the 2D CCHs.

Introduction

Colloidal crystals have attracted considerable attentions due to their applications in photonic crystals, nanoscale electronics, and optical sensors and displays.[1–12] Over the past several decades, research has been focused on the preparation of three-dimensional (3D) colloidal photonic crystals composed of monodisperse colloidal particles and their characterization and applications. However, just like homogeneous bulk semiconductor crystals, homogeneous photonic crystals on their own are quite limited in providing complex optical functions. More complex photonic crystal devices can be fabricated to produce more complex functionalities.[13–16] Artificial defects, such as point defects, line defects and planar defects, can be embedded into 3D colloidal crystals as "optical doping" to enrich their optical function.[13,17–19] Another approach to add functionality would fabricate colloidal crystal heterostructures (CCHs) that incorporate several different photonic structures into a single photonic crystal.

Recently, CCHs composed of colloidal crystals of different size monodisperse particles were used to increase the band width of photonic stop bands.[20–23] One approach to fabricate CCHs is to stack 3D colloidal crystal films along their optical axis. Several methods, such as Langmuir–Blodgett method,[24] vertical deposition process,[14] convective self-assembly scheme,[25] and controlled dip-coating method[26] have been used to prepare 3D CCHs. For example, Yan *et al.* prepared polymer opaline hetero photonic crystals using a convectional self-assembly and layer transfer technique.[23] Cai *et al.* fabricated a crack-free CCH by sequential convective self-assembly of polystyrene (PS) colloids.[20] Subsequent calcination of the opaline heterostructure formed inverse SiO_2 opaline heterostructures. The stop bands of these structures can be conveniently engineered by changing the lattice constant, which can be controlled in close packed arrays by adjusting the particle size. So far, almost all reported CCHs were fabricated in 3D colloidal crystals. In the work here, we present a simple and practical method for the fabrication of CCHs using two-dimensional (2D) colloidal monolayer crystals. Zhang *et al.* recently developed a air/water interface self-assembly method to fabricate 2D polystyrene colloidal arrays.[27–29] We utilized this method to prepare 2D poly(methyl methacrylate) (PMMA) colloidal particle arrays. These 2D colloidal arrays of PMMA particles can be formed in less than 1 min. These 2D colloidal arrays were transferred onto a substrate as the first layer of a 2D CCH. Subsequently, another 2D colloidal array with a different size PMMA particle was deposited on it to form a double layer 2D CCH. By repeating this procedure, a third layer was deposited to form a triple layer CCH. The integrity of the individual 2D CCHs was confirmed by SEM and optical diffraction. Compared to the conventional 3D CCHs, CCHs based on 2D colloidal crystals are much thinner and can be quickly

[a]*School of Chemical Engineering and Environment, Beijing Institute of Technology, Beijing, 100081, China. E-mail: m_zihui@yahoo.com; minxue@bit.edu.cn*

[b]*Department of Chemistry, University of Pittsburgh, Pittsburgh, PA 15260, USA. E-mail: asher@pitt.edu*

† Electronic supplementary information (ESI) available: Video of PMMA colloids self-assembly at the air/water interface. See DOI: 10.1039/c4ra16006a

fabricated at low cost. The process can be repeated to obtain any number of desired layers. The optical properties of these multilayers 2D arrays derive approximately from the diffraction of the individual layers.

Experimental

Preparation of monodisperse PMMA particles with different diameters

Monodisperse PMMA colloidal particles with a 262 nm diameter were prepared by using a previously reported emulsifier-free emulsion polymerization method.[30] These seed PMMA particles were washed thoroughly with deionized water and diluted with water to give a final concentration of 0.03 g mL^{-1}.

PMMA particles with larger sizes ranging from 420–748 nm were prepared by a seeded emulsifier-free emulsion polymerization method. Briefly, 25 mL of the seed PMMA suspension solutions were added to 90 mL deionized water in a four-neck round-bottom flask with a condenser. The solution was deoxygenated by bubbling with nitrogen for half an hour. The solution was then heated to 80 °C followed by injections of a 5 mL potassium peroxydisulfate solution (0.2 g) and the desired amount of MMA (1, 5, 10, 15 and 20 mL) was added through a side neck of the flask. A temperature sensor monitored the reaction temperature. The mixture was then refluxed for 45 min while being stirred at 300 rpm. After polymerization, the monodisperse PMMA particles of 420, 523, 626, 673, and 748 nm in diameter were washed with deionized water. Particle sizes were measured using scanning electron microscope (SEM, Quanta FEG 250).

Self-assembly of 2D colloidal monolayer array of PMMA particles

Common glass slides (Weiss Experiment Products Co. Ltd.) (22 × 22 × 0.15 mm) were used in this research. The glass slides were immersed in a H_2SO_4–H_2O_2 mixture (7 : 3) for 12 h, and then rinsed with deionized water in an ultrasonic bath for three times and then dried for use. The resultant PMMA particles were diluted with water to obtain a 0.15 g mL^{-1} suspension. The PMMA suspension was mixed with propanol at a ratio of 3 : 1 in volume, vortexed for 1 min and deposited on a water surface in a 10 cm diameter glass container where they formed a hexagonal close-packed 2D monolayer arrays. The water container was not subjected to any treating including heating. To transfer the 2D monolayer array onto a substrate, we lifted up the pre-placed glass slide and deposited the 2D array on the glass substrate.

Preparation of 2D CCHs

A 2D monolayer array was prepared from 626 nm PMMA colloidal particles and transferred onto a glass substrate. A double-layer 626–748 nm 2D CCH was fabricated by depositing a second 2D array of 748 nm PMMA particles onto the 626 nm monolayer array. Typically, we submerged the prepared 626 nm PMMA 2D monolayer array on the glass slide into water in order to lift and attach the 748 nm 2D array. Thus, the 748 nm 2D array was transferred onto the 626 nm 2D array.

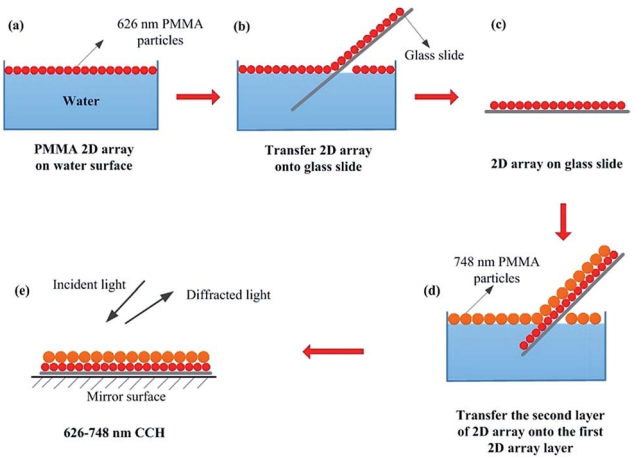

Fig. 1 Schematic illustration of the preparation of 2D CCHs.

A triple layer 523–626–748 nm 2D CCH was prepared similarly by sequentially depositing two 2D arrays of 626 nm and 748 nm PMMA particles on a 523 nm monolayer array surface. The CCHs fabrication process is schematically shown in Fig. 1.

Characterization of 2D CCHs

Gold layers were sputtered onto the resultant 2D CCHs. The particles, their orderings and morphologies were examined with an SEM (Quanta FEG 250, FEI). The optical diffraction of the 2D CCHs were measured at a 30° angle with a fiber optic UV-vis spectrometer (Avaspec-2048TEC, Avantes). Debye diffraction rings were measured to characterize the forward light diffraction of the 2D colloidal arrays and 2D CCHs.[31] A 405 nm violet-blue laser pointer illuminated the surface of the 2D CCA or 2D CCHs at normal incidence. The photographs of the CCHs were taken using a digital camera at an angle of ~30° between the light source/camera and the CCHs normal. The 2D CCHs were placed on an aluminum mirror.

Results and discussion

Preparation of PMMA particles with different diameters

The ordering of the 2D colloidal arrays decrease as the particle size decreases probably because the thinner particle arrays are less robust and they disorder during the sample handling.[28] 2D colloidal arrays of larger size (500–1000 nm) particles exhibit visible diffraction color.[28,31] We previously reported the preparation of PMMA particles between 150–280 nm by an emulsifier-free emulsion polymerization method.[30] However, the method is not suitable for the preparation of PMMA particles with diameters over ~400 nm. In the present work, PMMA particles in the range of 420–748 nm were prepared by a seeded polymerization method. Monodisperse PMMA seed particles with diameters of 262 nm were synthesized by the conventional emulsifier-free emulsion polymerization method. These seed particles were further grown to produce larger PMMA particles. Particles with diameters of 420, 523, 626, 673, and 748 nm were obtained by varying the amount of MMA monomer added as listed in Table 1. Their SEM images are shown in Fig. 2.

Table 1 Recipes for larger size PMMA particles[a]

PMMA seed suspension (mL)	MMA (mL)	KPS (g)	Diameter (nm)	Relative standard deviations
25	1	0.2	420	3.1%
25	5	0.2	523	2.9%
25	10	0.2	626	3.4%
25	15	0.2	673	2.2%
25	20	0.2	748	2.3%

[a] The concentration of the PMMA seed suspension was 0.03 g mL^{-1}.

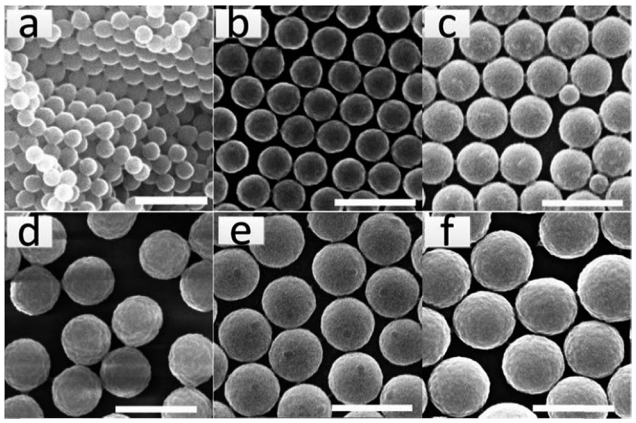

Fig. 2 SEM images of monodisperse PMMA particles with diameters of 262 (a), 420 (b), 523 (c), 626 (d), 673 (e), and 748 nm (f). The scale bars are 1 μm in length.

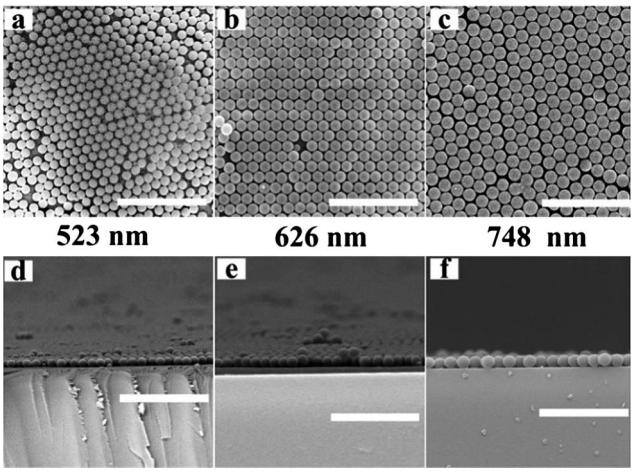

Fig. 3 SEM images of 2D colloidal monolayer arrays of PMMA particles of 523 (a and d), 626 (b and e), 748 diameters nm (c and f). a, b and c are in-plane SEM images of PMMA 2D arrays, and d, e and f SEM images show the cross-section of PMMA 2D array monolayers. The scale bars are 5 μm in length.

Self-assembly of 2D colloidal monolayer arrays with different sizes of PMMA particles

An aqueous 1-propanol-containing a colloidal particle suspension rapidly assembles into a hexagonal close-packed 2D colloidal monolayer array at the air/water interface in a manner similar to that reported by Zhang *et al.*[28] In Zhang's research, for the self-assembly of PS latex particles on a water surface using a water/1-propanol solvent, a continuous 2D colloidal monolayer array of an area >280 cm^2 was prepared within 2 min.[28]

Methanol, ethanol, propanol, and isopropanol were tested for use in preparing PMMA 2D colloidal arrays. A 3 : 1 ratio by volume of a PMMA particle suspension (0.15 g mL^{-1}) to 1-propanol gave the best results. When the 1-propanol-containing PMMA colloidal suspension was gently layered on the water surface the PMMA particles quickly spread due to the Marangoni effect, *e.g.* the surface tension gradient on the water surface spreads the PMMA suspension. As the colloidal particles spread outward, they self-assemble rapidly into a hexagonal close-packed 2D monolayer array (see ESI†). The floating 2D array was transferred onto a glass slide as shown in Fig. 1b by lifting the substrate from beneath the water. In the present work, 523, 626, 673, and 748 nm PMMA particles were ordered into hexagonal 2D monolayer arrays, as confirmed by their SEM images (Fig. 3).

Because the 2D array monolayer has spacings of the order of hundreds of nanometers, the resulting structure strongly diffracts visible light. For incident light normally incident to the array the diffraction, follow Bragg's law:

$$m\lambda = \sqrt{3}d \sin\theta, \quad (1)$$

where m is the diffraction order, λ is the diffracted wavelength in air, d is the 2D particle spacing, and θ is the angle between the propagation direction of the diffracted light and the normal to the 2D array.[32] Both θ and d were adjusted to obtain diffraction in the visible spectral region. 2D monolayer arrays show strong forward diffraction that can be easily monitored by using a mirror to back reflect the forward diffracted light.[28,32,33] We used a front surface mirror to reflect the forward diffraction. The intense back diffracted light could easily be observed by illuminating the 2D array with a flashlight.

The optical back diffraction wavelength of the 2D CCHs were measured at a 30° angle with a fiber optic UV-vis spectrometer in the Littrow configuration. The diffraction spectrum of 2D arrays of 523 nm, 626 nm, 673 nm and 748 nm PMMA particles are shown in Fig. 4a. The diffraction peak red-shifts from 470 nm to 621 nm as the particle diameter increases from 523 to 748 nm. This red-shift obeys the 2D photonic crystal Bragg diffraction law.

The back-diffracted color was photographed at a 30° angle between the light source/camera and the 2D array normal (Fig. 4b). It red-shifts from blue to green, to yellow, and to red with increasing particle size from 523 to 748 nm. The diffraction

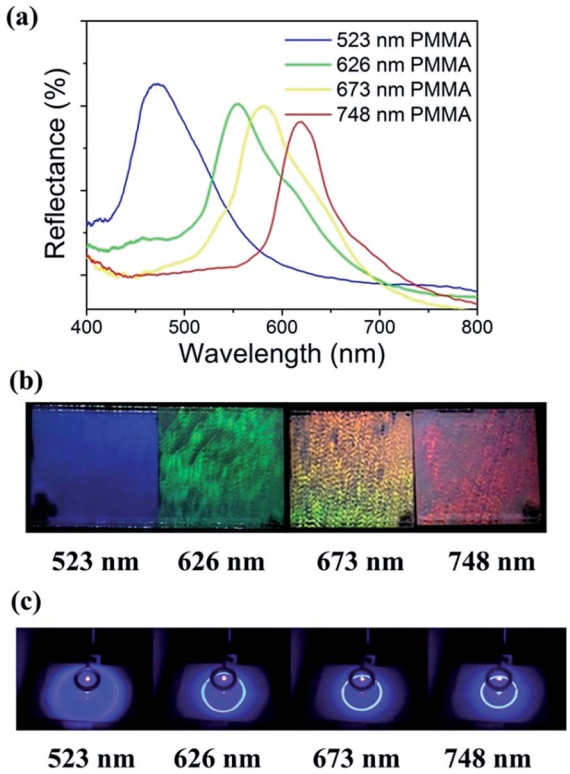

Fig. 4 (a) Diffraction spectra measured in Littrow configuration of 2D monolayer arrays of PMMA particles with diameters of 523, 626, 673 and 748 nm on a mirror. (b) Photograph of diffracted color of forward diffracted white light at 30 degrees from the normal, and (c) Debye diffraction ring.

wavelength and the diffraction angles can be controlled by varying the particle diameter in these close-packed 2D arrays.

The strong forward light diffraction of the 2D colloidal monolayer array results in a Debye diffraction ring if the array is illuminated along the normal by monochromatic light.[31] The Debye diffraction of the 2D colloidal array follows eqn (2):

$$\sin \alpha = 2\lambda \Big/ \sqrt{3}d, \quad (2)$$

where α is the forward diffraction angle of the Debye diffraction, λ is the incident wavelength in air, and d is the particle spacing. Diffraction by a perfectly ordered 2D array results in the diffraction of a hexagonal array of Bragg spots. However, the randomly oriented small ~20 μm crystallites of the hexagonally ordered the 2D array scatter the diffracted light into a ring.[25] The forward diffraction angle, α, is $\alpha = \text{arc tan } D/2h$, where h is the distance between 2D array and the screen, and D is the diameter of the Debye diffraction ring. Therefore, the 2D array particle spacing can be determined simply by measuring the diameter D of the Debye ring.

Fig. 4c shows the Debye diffraction rings of the 523, 626, 673, and 748 nm particle diameter 2D colloidal arrays that show diameters of 19.5, 13.2, 12.0 and 10.9 cm, respectively. The Debye ring diameter decreases with increasing particle size. The Debye diffraction intensity of 523 nm 2D array is much weaker than those of the other three 2D arrays of larger particles. Part of the reason is the decreased scattering for smaller particles. Another reason might be that 523 nm layer has poorer ordering. In addition, the 2D colloidal array with smaller PMMA particles gives a larger forward diffraction angle, which increases the width of the diffraction ring decreasing the irradiance. Thus, the brightness of the diffraction ring decreases on the screen. According to eqn (2), the corresponding particle spacing are 578, 685, 722, 766 nm. It is noted that the calculated particle spacing of the 2D arrays are ~40 nm larger than the PMMA particle diameters. This might occur because the colloids are not exactly close-packed, which is consistent with the (Fig. 2) by SEM images.

Preparation and characterization of PMMA 2D CCHs

A 2D monolayer array of 626 nm PMMA particles were attached to a glass slide as described above. Another 2D monolayer array of 748 nm PMMA particles was then transferred onto the 626 nm PMMA 2D colloidal array surface. This double-layer 2D CCH is denoted as a 626–748 nm 2D CCH. The first 2D array monolayer array of 626 nm PMMA particles firmly attaches to the glass slide to provide a relatively flat surface for placement of the second 2D array. The Fig. 5 SEM images clearly show the stacked two monolayer array layers.

The 626–748 nm 2D CCH was prepared by depositing an array of larger PMMA particles on the smaller PMMA particles. When the array of smaller spheres is transferred onto the larger spheres, the smaller spheres could sag into the interstices of the larger spheres at their interface and its ordering degraded.[14,24] To determine if there is a dependence of ordering on size ordering of the stacked layers a 748–626 nm 2D CCH was prepared by depositing a 2D array of 626 nm PMMA particles onto the other 2D array of 748 nm particles. Its SEM top-view image shows that the top-layered 626 nm 2D monolayer array maintains its original structural integrity (Fig. 5c). The cross-sectional SEM image in Fig. 5d demonstrates the well-aligned

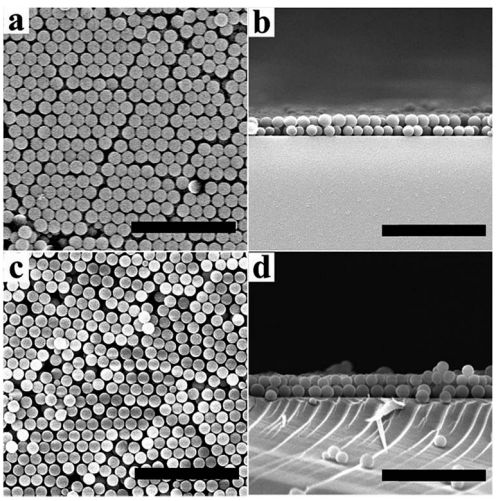

Fig. 5 SEM images of the CCHs composed of stacked 2D colloidal arrays. (a) and (b) are the top-view SEM image and cross-sectional SEM image of the 626–748 nm CCH. (c) and (d) are the plane-view SEM image and cross-sectional SEM image of 748–626 nm CCH. The scale bars are 5 μm long.

two PMMA 2D array layers. Thus, the particle size and ordering of the two monolayer arrays do not effect the integrity of the resultant 2D CCHs.

The reflectance spectra of the 626–748 nm 2D CCH, 748–626 nm 2D CCH and their corresponding monolayer arrays are shown in Fig. 6a and b. The 626–748 nm 2D CCH exhibits two overlapping diffraction peaks centered at ~559 nm and ~696 nm (black line in Fig. 6a). The diffraction peak positions of the 2D CCH correspond to the diffraction peaks of the individual 626 nm and 748 nm 2D monolayer arrays. The 748–626 nm 2D CCH shows similar diffraction spectra, that derives from the diffraction of the individual 2D colloidal arrays (Fig. 6b). We conclude that the optical properties of these multilayers 2D arrays mainly derive from the sum of the diffraction of the individual two 2D array layers. However, there is an increased diffraction that appears on the short wavelength edge. The 626–748 nm 2D CCH also exhibits Debye diffraction rings under monochromatic light illumination (Fig. 6c). Two individual Debye diffraction rings with diameters of 13.2 cm and 10.9 cm were observed from the 626 nm and 748 nm 2D monolayer arrays, respectively. In addition, the diffracted color of the 626–748 nm 2D CCH is a combination of the green and red diffraction which is attributed to the 626 nm and 748 nm 2D monolayer arrays, respectively (Fig. 6d). The diffracted color photograph were taken at an angle of 30° between the light source/camera and the CCHs normal. Thus, the 2D CCHs diffraction appears to be the sum of the diffraction from the individual 2D colloidal arrays. This enables the combining of different diffracted light wavelengths.

A 523–626–748 nm 2D CCH and a CCH with reverse layer stacking, 748–626–523 2D CCH were prepared by using the colloidal array transfer method. Their cross-sectional SEM images show that both maintain a structural integrity (Fig. 7a and b). Their combined diffraction bands are broad due to the overlapped diffraction of the individual 2D monolayer arrays (Fig. 7c and d). Three Debye diffraction rings were observed under monochromic light illumination (Fig. 7e). Two bright rings with diameter of 10.9 and 13.2 cm are attributed to the 748 nm and 626 nm 2D monolayer arrays, respectively. The third weak Debye diffraction ring with a diameter of 19.5 cm is from the 523 nm 2D monolayer array, showing the weak Debye diffraction ring of the 523 nm 2D monolayer array alone under the same illumination (Fig. 4c). In addition, diffraction from the three layer periodicity could further reduce the 2D diffraction intensity. Blue, green and red diffraction colors of the 523–626–748 nm 2D CCH can be observed for the light source and camera at an angle of 30° to the CCHs normal (Fig. 7f).

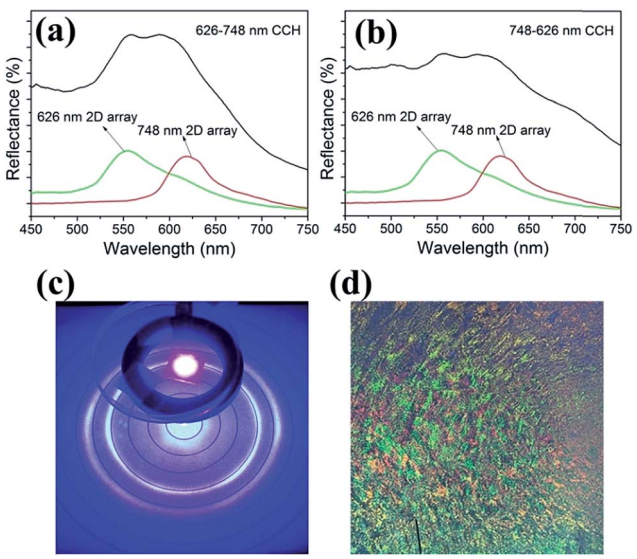

Fig. 6 Reflectance spectra in a Littrow configuration (a) of the 626–748 nm 2D CCH and (b) 748–626 nm 2D CCH. The reflectance spectra of a 626 nm and 748 nm 2D monolayer array are also included for the comparison. (c) Two Debye diffraction rings of the 626–748 nm 2D CCH photographed from a screen (c). Photograph of diffraction color of the 626–748 nm 2D CCH shows both green and red diffraction (d).

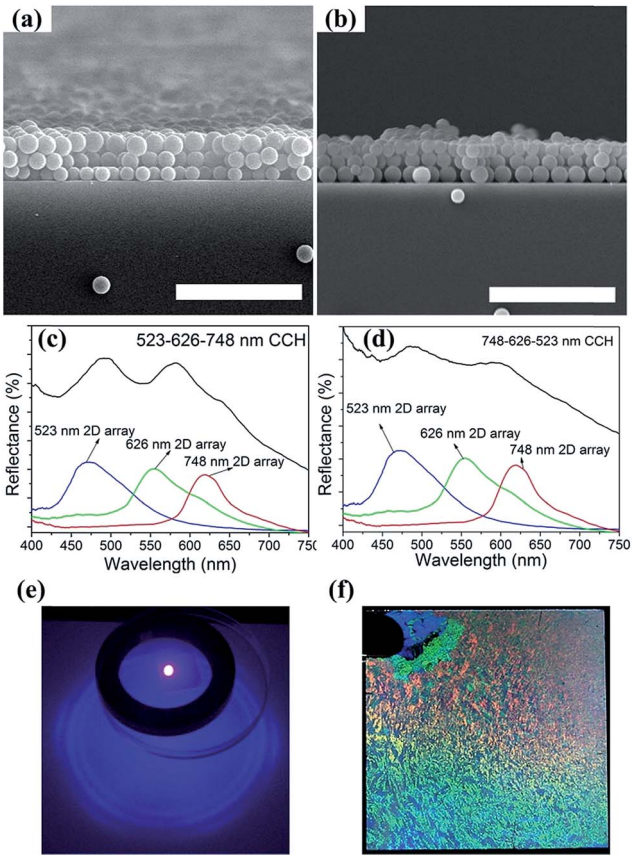

Fig. 7 Cross-sectional SEM images of (a) 523–626–748 nm and (b) 748–626–523 nm 2D CCHs. Diffraction spectra at the Littrow condition of (c) 523–626–748 nm and (d) 748–626–523 nm 2D CCHs. Debye rings obtained under the illumination with a 405 nm violet-blue laser beam. Three Debye diffraction rings were observed on the screen. (f) The diffraction color of the 523–626–748 nm 2D CCH shows blue, green and red light. The scale bars is 5 μm long.

Conclusions

Double-layer and triple-layer CCHs composed of 2D colloidal arrays of PMMA particles with different diameters were fabricated using successive deposition of 2D colloidal monolayer arrays prepared at the air/water interface. We characterized the

CCHs ordering by measuring the diffraction spectrum, the Debye diffraction ring, and the diffraction color. Both structural observation and optical characterization confirm the good ordering of the resultant opaline heterostructures. The resulting CCHs exhibit optical properties that are similar to the expected superposition of diffraction of the individual 2D colloidal monolayer arrays. Thus, diffraction property can be designed by varying the spacing of the array of PMMA colloidal particles. These multilayer structures afford new opportunities for engineering photonic crystal diffraction which may have important applications in optical filters, reflectors, waveguides, *etc.*

Acknowledgements

This research was supported by NSFC (21375009, to ZM) and HDTRA (grant no. 1-10-1-0044, to SA). We also gratefully thank the Graduate School in Beijing Institute of Technology for the Joint PhD Student Scholarship Program.

Notes and references

1 F. Li, D. P. Josephson and A. Stein, *Angew. Chem., Int. Ed.*, 2010, **50**, 360–388.
2 G. von Freymann, V. Kitaev, B. V. Lotsch and G. A. Ozin, *Chem. Soc. Rev.*, 2013, **42**, 2528–2554.
3 C. Fenzl, T. Hirsch and O. S. Wolfbeis, *Angew. Chem., Int. Ed.*, 2014, **53**, 3318–3335.
4 D. Yang, S. Ye and J. Ge, *Adv. Funct. Mater.*, 2014, **24**, 3197–3205.
5 C. G. Schäfer, M. Biesalski, G. P. Hellmann, M. Rehahn and M. Gallei, *J. Nanophotonics*, 2013, **7**, 070599.
6 C. G. Schäfer, C. Lederle, K. Zentel, B. Stühn and M. Gallei, *Macromol. Rapid Commun.*, 2014, **35**, 1852–1860.
7 L. González-Urbina, K. Baert, B. Kolaric, J. Pérez-Moreno and K. Clays, *Chem. Rev.*, 2011, **112**, 2268–2285.
8 J. Ge and Y. Yin, *Angew. Chem., Int. Ed.*, 2010, **26**, 18357–18361.
9 M. Bardosova, M. E. Pemble, I. M. Povey and R. H. Tredgold, *Adv. Mater.*, 2010, **22**, 3104–3124.
10 C. Geng, T. Wei, X. Wang, D. Shen, Z. Hao and Q. Yan, *Small*, 2014, **10**, 1668–1686.
11 Y. Zhang, J. Wang, Y. Huang, Y. Song and L. Jiang, *J. Mater. Chem.*, 2011, **21**, 14113–14126.
12 M. Kumoda, M. Watanabe and Y. Takeoka, *Langmuir*, 2006, **22**, 4403–4407.
13 Q. Yan, L. Wang and X. S. Zhao, *Adv. Funct. Mater.*, 2007, **17**, 3695–3706.
14 S. Wong, V. Kitaev and G. A. Ozin, *J. Am. Chem. Soc.*, 2003, **125**, 15589–15598.
15 L. K. Teh, Q. Yan and C. C. Wong, *ACS Appl. Mater. Interfaces*, 2009, **1**, 775–779.
16 P. Massé, R. A. L. Vallée, J.-F. o. Dechézelles, J. Rosselgong, E. Cloutet, H. Cramail, X. S. Zhao and S. Ravaine, *J. Phys. Chem. C*, 2009, **113**, 14487–14492.
17 K. Wostyn, Y. Zhao, G. de Schaetzen, L. Hellemans, N. Matsuda, K. Clays and A. Persoons, *Langmuir*, 2003, **19**, 4465–4468.
18 Y. Zhao, K. Wostyn, G. d. Schaetzen, K. Clays, L. Hellemans, A. Persoons, M. Szekeres and R. A. Schoonheydt, *Appl. Phys. Lett.*, 2003, **82**, 3764–3766.
19 P. V. Braun, S. A. Rinne and F. García-Santamaría, *Adv. Mater.*, 2006, **18**, 2665–2678.
20 Z. Cai, Y. J. Liu, J. Teng and X. Lu, *ACS Appl. Mater. Interfaces*, 2012, **4**, 5562–5569.
21 C. Zhang, F. Qiao, J. Wan and J. Zi, *J. Appl. Phys.*, 2000, **87**, 3174–3176.
22 Q. Yan, X. S. Zhao and Z. Zhou, *J. Cryst. Growth*, 2006, **288**, 205–208.
23 Q. Yan, L. K. Teh, Q. Shao, C. C. Wong and Y.-M. Chiang, *Langmuir*, 2008, **24**, 1796–1800.
24 M. Bardosova, M. E. Pemble, I. M. Povey, R. H. Tredgold and D. E. Whitehead, *Appl. Phys. Lett.*, 2006, **89**, 093116.
25 R. V. Nair and R. Vijaya, *J. Appl. Phys.*, 2007, **102**, 056102.
26 M. Egen, R. Voss, B. Griesebock, R. Zentel, S. Romanov and C. S. Torres, *Chem. Mater.*, 2003, **15**, 3786–3792.
27 J.-T. Zhang, L. Wang, X. Chao and S. A. Asher, *Langmuir*, 2011, **27**, 15230–15235.
28 J.-T. Zhang, L. Wang, D. N. Lamont, S. S. Velankar and S. A. Asher, *Angew. Chem., Int. Ed.*, 2012, **51**, 6117–6120.
29 J.-T. Zhang, L. Wang, X. Chao, S. S. Velankar and S. A. Asher, *J. Mater. Chem. C*, 2013, **1**, 6099–6102.
30 F. Xue, Z. Meng, Y. Wang, S. Huang, Q. Wang, W. Lu and M. Xue, *Anal. Methods*, 2014, **6**, 831–837.
31 J.-T. Zhang, X. Chao, X. Liu and S. A. Asher, *Chem. Commun.*, 2013, **49**, 6337–6339.
32 J.-T. Zhang, L. Wang, J. Luo, A. Tikhonov, N. Kornienko and S. A. Asher, *J. Am. Chem. Soc.*, 2011, **133**, 9152–9155.
33 A. Tikhonov, N. Kornienko, J.-T. Zhang, L. Wang and S. A. Asher, *J. Nanophotonics*, 2012, **6**, 063509.

